



FUSION

OAK RIDGE NATIONAL LABORATORY LIBRARIES



3 4456 0539398 1

ORNL/Sub-79/21453/6

cy. 22

FED LIBRARY AUG 4 1981

60 GHz GYROTRON DEVELOPMENT PROGRAM

J.F. Shively, M.K. Cheng, S.E. Evans,
T.J. Grant and D.S. Stone

Quarterly Report No. 6
October through December 1980

Prepared for:

OAK RIDGE NATIONAL LABORATORY
OAK RIDGE, TENNESSEE 37830

Operated by:

UNION CARBIDE CORPORATION
FOR THE DEPARTMENT OF ENERGY

CONTRACT NO. W-7405-ENG-26

Varian Associates, Inc.
Palo Alto Microwave Tube Division
611 Hansen Way
Palo Alto, California 94303

OAK RIDGE NATIONAL LABORATORY LIBRARIES



3 4456 0536807 2

Printed in the United States of America. Available from
National Technical Information Service
U.S. Department of Commerce
5285 Port Royal Road, Springfield, Virginia 22161
NTIS price codes—Printed Copy: A04 Microfiche A01

This report was prepared as an account of work sponsored by an agency of the United States Government. Neither the United States Government nor any agency thereof, nor any of their employees, makes any warranty, express or implied, or assumes any legal liability or responsibility for the accuracy, completeness, or usefulness of any information, apparatus, product, or process disclosed, or represents that its use would not infringe privately owned rights. Reference herein to any specific commercial product, process, or service by trade name, trademark, manufacturer, or otherwise, does not necessarily constitute or imply its endorsement, recommendation, or favoring by the United States Government or any agency thereof. The views and opinions of authors expressed herein do not necessarily state or reflect those of the United States Government or any agency thereof.

60 GHz GYROTRON DEVELOPMENT PROGRAM

J.F. Shively, M.K. Cheng, S.E. Evans
T.J. Grant and D.S. Stone

Quarterly Report No. 6
October through December 1980

Prepared for:
Oak Ridge National Laboratory
Oak Ridge, Tennessee 37830

Operated by:
Union Carbide Corporation
For the Department of Energy

Contract No. W-7405-ENG-26

Varian Associates, Inc.
Palo Alto Microwave Tube Division
611 Hansen Way
Palo Alto, California 94303

ABSTRACT

The objective of this program is to develop a microwave oscillator capable of producing 200 kW of CW output power at 60 GHz. The use of cyclotron resonance interaction is being pursued.

The design, procurement and construction phases of this program are discussed.

Progress on gyrotron behavior studies being performed at 28 GHz are also discussed.

TABLE OF CONTENTS

<u>Section</u>	<u>Page</u>
I. INTRODUCTION	1
II. GYROTRON BEHAVIOR STUDY	2
A. Arcing and Crowbar Investigation	2
B. Voltage Gradients and Trapped Electrons Computer Investigation	3
C. Process and Bakeout	3
D. RF Behavior	4
E. Cavity and Output Taper	4
III. ELECTRON GUN	8
IV. SUPERCONDUCTING SOLENOID MAGNET	9
V. ANODE	10
VI. COLLECTOR	16
VII. WINDOW	27
VIII. COMPONENTS	31
A. Waterloads	31
B. Frequency Sampler and Arc Detector	31
C. Mode Filters	31
D. Miter Band	34
E. Flange Adapters	34
IX. TUBE ASSEMBLY	35
A. VGE-8060X1	35
B. VGE-8060S1	35
C. VGE-8060S2	35
X. PROGRAM SCHEDULE AND PLANS	36
XI. REFERENCES	43

LIST OF ILLUSTRATIONS

<u>Figure</u>		<u>Page</u>
1.	Optimized Power vs Gun Anode Voltage	5
2.	Power vs Main Magnet Current	6
3.	Power vs Gun Coil #1 Current	7
4.	Load Ring Assembly	11
5.	Cross Section of Brazed Assembly	12
6.	Cracked Surfaces After Thermal Cycling	14
7.	Infinitely Thick Slab	17
8.	Slab of Finite Thickness	20
9.	Roots of $\cot y = \frac{Y}{B}$	22
10.	Transient Temperature Profiles in Collector Wall .	24
11.	Pulse Duration Regimes For Gyrotron Collectors ...	26
12.	Window Cold Test Arrangements	28
13.	Ceramics Disc	29
14.	Pulsed Waterload	32
15.	Outline VCE-8006A1 Frequency Sampler and Arc Detector	33
16.	Milestone Chart	37

I. INTRODUCTION

The objective of this program is to develop a microwave oscillator designed to produce 200 kW of CW output power at 60 GHz. Neither tunability nor bandwidth are considered important parameters in the design but efficiency is. Mode purity in the output waveguide is not a requirement for the device, but the circular electric mode is considered desirable because of its low loss properties.

With these objectives in mind, an approach based on cyclotron resonance interaction between an electron beam and microwave fields is being pursued. The detailed arguments leading to this approach are contained in the final report of a preceding study program¹. The device configurations of particular interest, called gyrotrons, have been discussed in recent literature²⁻⁶. They employ a hollow electron beam interacting with cylindrical resonators of the TE_{0M1} class.

The optimum beam for the cyclotron resonance interaction is one in which the electrons have most of their energy in velocities perpendicular to the axial magnetic field. Another requirement is that the spread in the axial components of the electron velocities be as small as possible. Electrons which have different axial velocities will not interact efficiently.

The approach chosen to generate the beam is a magnetron type of gun as is used on the 28 GHz gyrotron, also developed for Oak Ridge National Laboratory^{7,8}. With this type of gun the shaping of the magnetic field in the gun region becomes quite important.

Construction of the experimental pulsed 60 GHz gyrotron is continuing. The first tube is ready for the pump. Evacuation and bakeout will commence January 6. The superconducting solenoid magnet system, from Magnetic Corporation of America, was received at Varian on December 30. At present, the limiting item appears to be modification of the test set.

II. GYROTRON BEHAVIOR STUDY

A. ARCING AND CROWBAR INVESTIGATION

A majority of the quarter was spent working with various tubes and trying to find a cause for the frequent crowbars in the VGA-8000 and VGA-8050 tubes. The purpose of this work is to eliminate some of the design problems in gyrotrons so the developmental work at higher frequencies can proceed more rapidly.

A table of probable events that would occur with different types of faults was formulated. This will enable the characterization of faults. To help in this matter, a capacitive divider was put in the cathode voltage line to see how the cathode voltage fluctuates around the time of a crowbar.

Different types of oscilloscopes were used to try to determine the timing between parameters such as gun anode current and cathode current. The timing difference between these two currents at crowbar is usually undetectable. Many crowbars were observed, and in 98% of the cases the crowbar occurred during the pulse. Only a few interpulse crowbars were observed. It was also seen that the crowbars occurred only when there was some amount of beam current. Most of the crowbars were very similar in their characteristics. Some observations were that the timing of various current increases and voltage decreases were the same time after time and the amplitudes of current were always about the same. Most of the fault current is seen in the collector and not in the body. This would seem to indicate an upper seal arc.

Data were taken to see if there was any correlation between the cathode temperature and the frequency of crowbars. The data did not show any correlation.

Plans have been made to use some rf antennas to determine if there is any type of gun oscillation which could cause problems.

B. VOLTAGE GRADIENTS AND TRAPPED ELECTRONS - COMPUTER INVESTIGATION

Work was performed during the quarter to further investigate voltage gradients in the gun. The gradient from the gun anode was found to be 65 kV/cm when the tube is pulsed on and is 111 kV/cm when pulsed off. The gradient from the surface of the front focus electrode is 109 kV/cm when the tube is pulsed on and 74 kV/cm when the tube is pulsed off. These gradient values are acceptable but have very little safety factor. By moving the gun 0.3 inches away from the body, the gradients at the gun anode can be lowered to 92 kV/cm. Further work is necessary to see if this sort of movement is detrimental to beam quality.

Due to some sputtering of metals on the ceramic insulators of the gun, the possibility of ion bombardment of the tip of the focus electrode has been investigated. The computer codes show that any ions formed in the interaction region of the tube will indeed strike the front focus electrode. The diameter of the ion impact area is dependent on the atomic number of the ions. Chemical analysis of the material sputtered on the ceramics found all materials normally used in vacuum tubes. After exposure to the air, this coating is found to be non-conducting. Work is being done to identify materials that would be better for this environment.

Using the computer code, investigation has also been done on electrons which may be emitted from a surface other than the cathode and where they will go. Electrons emitted from the front focus electrode and anode will go down the drift tube, while those from the rear focus electrode will split and some will strike the anode and those remaining will go out the drift tube. None seem to stay for any appreciable time in the region of the gun.

C. PROCESS AND BAKEOUT

The test vehicle, VGA-8000 S/N 11, went through bakeout, and the cathode was processed. The bakeout time was doubled to try to release and eliminate more gas from the metal walls of the tube. The cathode processing consists of applying voltage and current to the heater. This tube has the K-8002 gun using different heater voltage and current, than the K-8000 gun.

The total time to age the tube in the socket was not established because of an error in cathode processing. The gun was processed to only 20 watts heater power when it should have been processed to 50 watts before being placed in the socket. This new bakeout schedule appears to have made an improvement in tube processing and will be used in future tubes.

D. RF BEHAVIOR

The VGA-8000 S/N8 was not operated with high level rf. The tube was then pulled and it was found to have a cracked output window. The crack appears to be due to over-pressure rather than any thermal or rf induced problem. More investigation is being performed.

The VGA-8000 S/N 11 was pulse tested to 200 kw peak power. This tube will be CW tested next quarter. Curves were taken to show the types of excursion possible in magnet currents and gun anode voltage (Figures 1-3).

Figure 1 shows the optimized power output at a given gun anode voltage. In Figure 1 the magnetic fields were varied to optimize the peak power output. Figure 2 is the peak output power variation for a given change in main magnetic field. The main magnetic current was lowered until the tube oscillated in a mode other than the TE_{021} . Figure 3 shows how the output power varies with gun coil magnet current. The tube is normally operated with no gun anode current being drawn. At 12.1 A of gun coil No. 1 current the gun anode began drawing current. Above 12.1 A there is no gun anode current.

E. CAVITY AND OUTPUT TAPER

Computer simulation has been used to design a new cavity and output taper for low mode conversion. The existing cavity, if used with the new output taper configuration, would have a Q less than 200. The new cavity and taper design has a Q of 430, which was used in the earlier 28 GHz work. Cold test work is being done to find the correlation between the cold test data and the computer simulation. This cavity will also have the TM mode detuning as used in the earlier 28 GHz work.

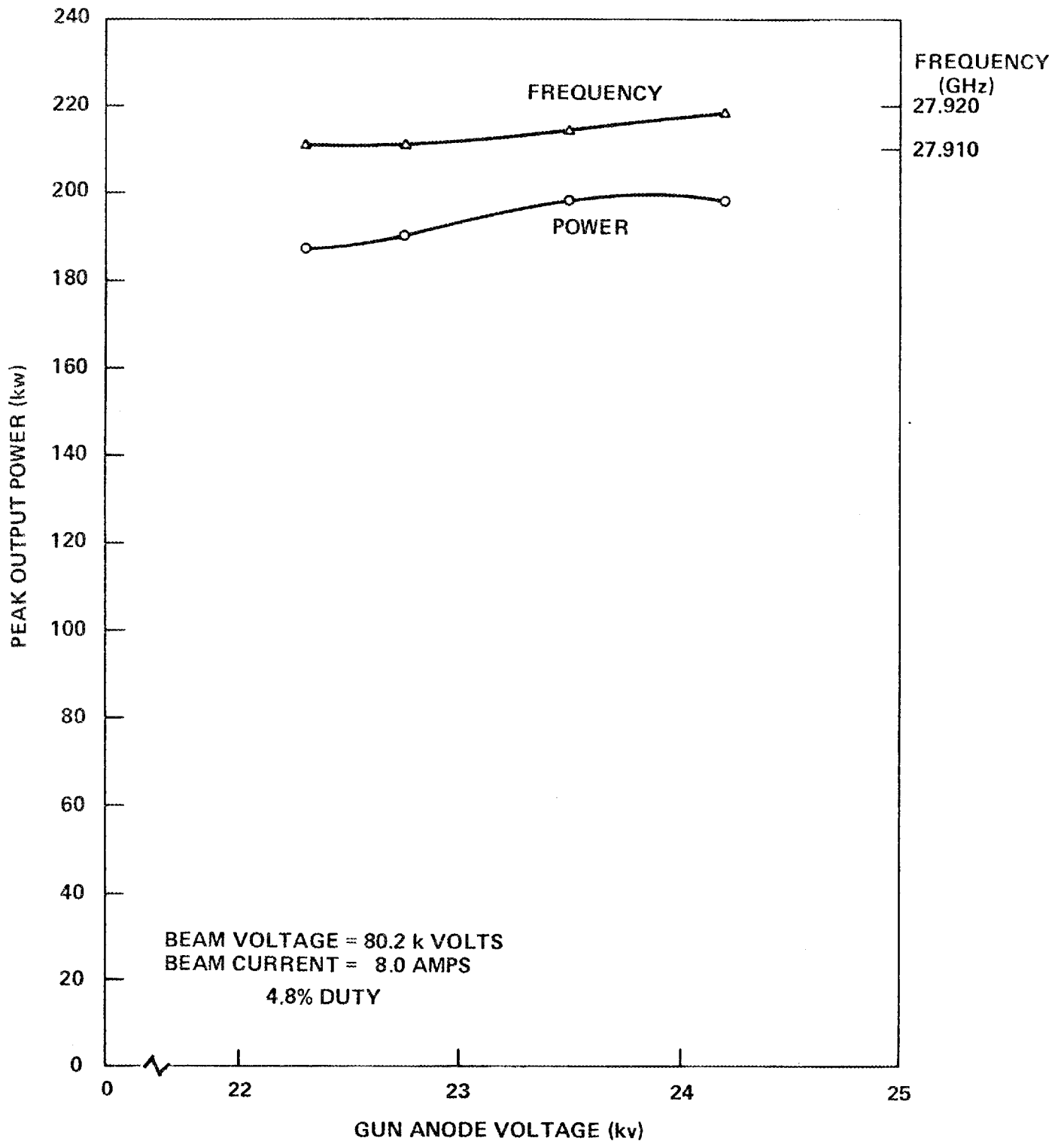


FIGURE 1. OPTIMIZED POWER vs GUN ANODE VOLTAGE

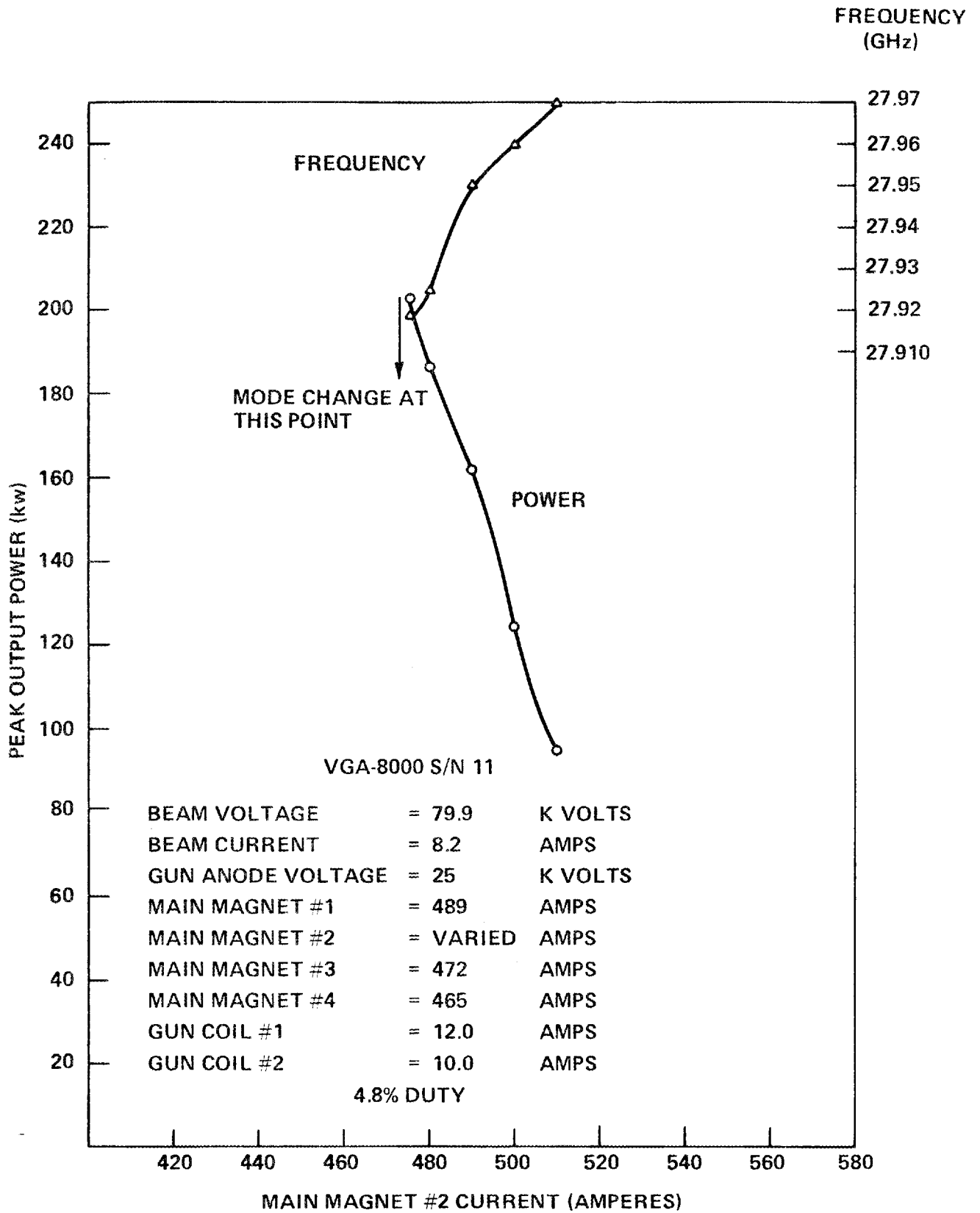


FIGURE 2. POWER vs MAIN MAGNET CURRENT

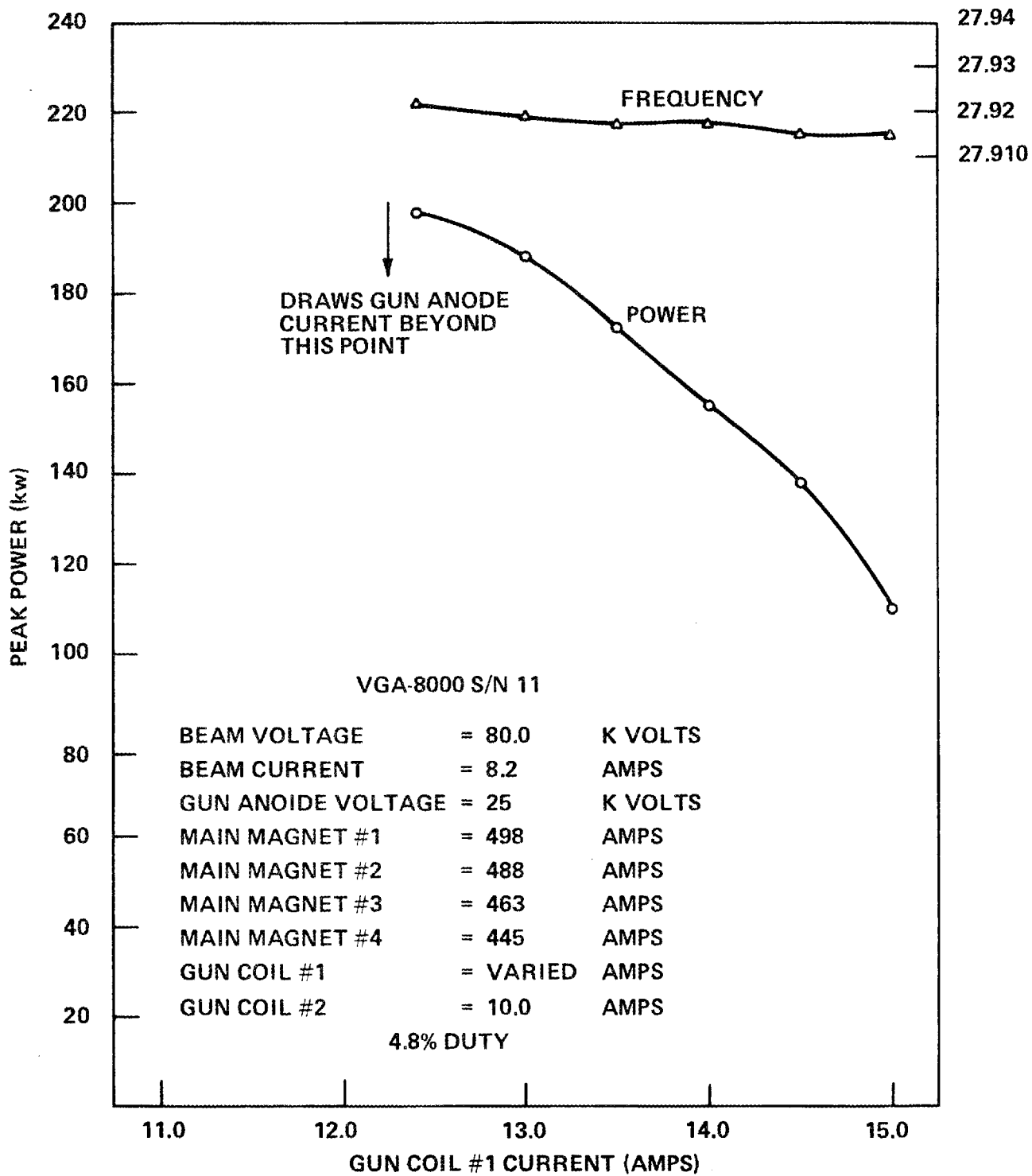


FIGURE 3. POWER vs GUN COIL #1 CURRENT

III. ELECTRON GUN

Several problems were overcome during the quarter in the assembly of the first electron gun for use on the experimental 60 GHz gyrotron, serial number X-1. A leak between the gun anode oil cooling channel and the vacuum required rework of the high voltage seal assembly. A heater lead which was broken during heater testing required rework of the final cathode stem assembly. A problem with brazing the cathode to its support structure necessitated remaking the piece parts after a rework failed. These problems delayed construction of the first gun until December.

A second gun, for use on the first 100 ms pulse duration gyrotron, model VGE-8060 serial number 1 is under construction. Parts for five additional guns are available.

IV. SUPERCONDUCTING SOLENOID MAGNET

Difficulty was encountered in winding the coils. In addition, an accident in magnet operation at Magnetic Corporation of America resulted in a partial short in one of the main coils, requiring coil repair and rewinding. Testing of the superconducting solenoid magnet system was completed at Magnetic Corporation of America in December. The system was received at Varian on December 30. Installation is scheduled for early January.

V. ANODE

During the quarter, a variety of braze joints used in the ceramic anode subassemblies were tested for strength, bonding uniformity, and ability to withstand the thermal cycling of subsequent brazing operations. These subassemblies require a bond between the faces of a silicon carbide loaded beryllia washer and thin copper caps (see Figure 4). For the fabrication trials, two of the most appropriate Varian active metal braze processes were selected. These require excellent surface contact between the copper caps, the ceramic, and the active metal braze material. The braze fixture is designed to guarantee the good surface contact by taking advantage of differential expansion between the jig and the assembly to hold the joint under compression at braze temperature.

The anode subassembly shown in Figure 4 represents a particularly difficult application of this technique because of the large differential radial expansion between the ceramic and the copper. Once the braze joint is formed at high temperature, the differential radial contraction (approximately 0.014") during cooldown tends to shear the joint. If the joint is initially strong but brittle, then during cooldown either the joint or the ceramic will crack under shear. If on the other hand a weaker but more ductile bond is employed, the shear can be relieved by the elasticity of the joint. In spite of the disadvantage of lower strength, the ductile joint was chosen for the mode subassemblies because of its resistance to cracking even after repeated thermal cycling.

In order to check the metallurgical quality of the braze joints in the test samples, a cross section of the brazed assembly was examined with the scanning electron microscope for the active metal, silicon, and copper (see Figure 5). No sign of excessive active metal migration into the copper or the ceramic was evident; no diffusion of silicon into the copper cup was found either. These scans indicate that the assemblies were not brazed for excessive time and/or at excessive temperature and that the active metal braze joints were properly formed.

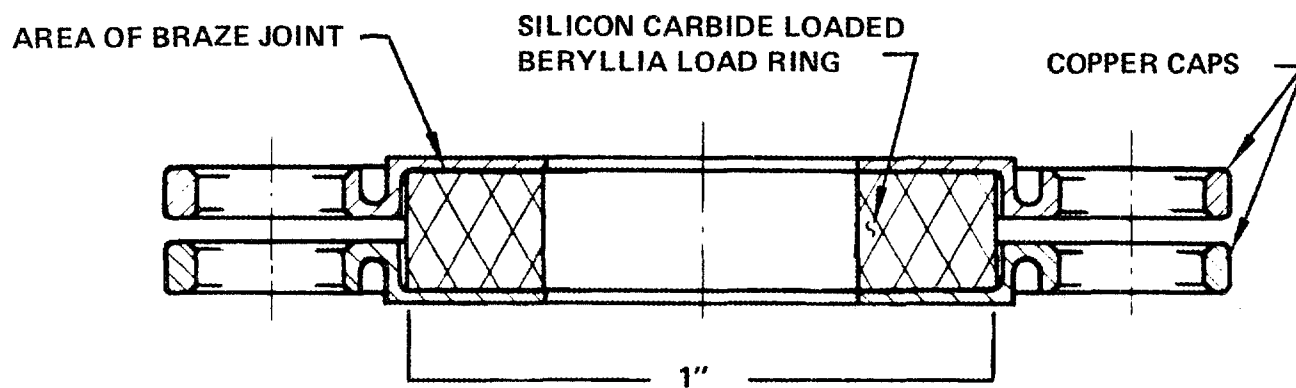


FIGURE 4. LOAD RING ASSEMBLY

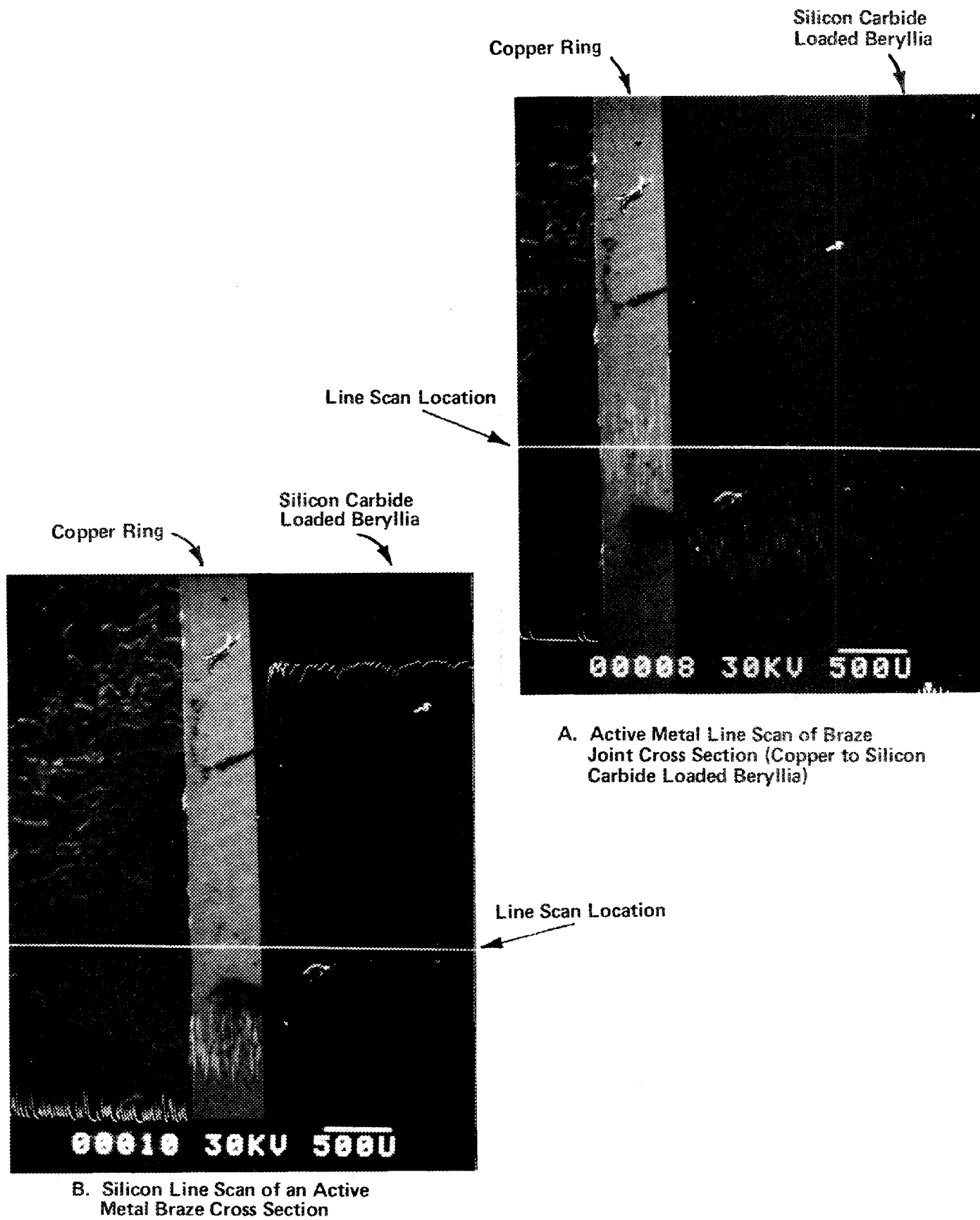


FIGURE 5. CROSS SECTION OF BRAZED ASSEMBLY

The strength of the braze joints was determined by peel testing. The assemblies were cut into semicircular halves and the copper cups were peeled off. The peel strength was then determined according to

$$\text{Peel strength (lb/in)} = \frac{\text{Peel force (lb)}}{\text{Width of peel strip (in)}}$$

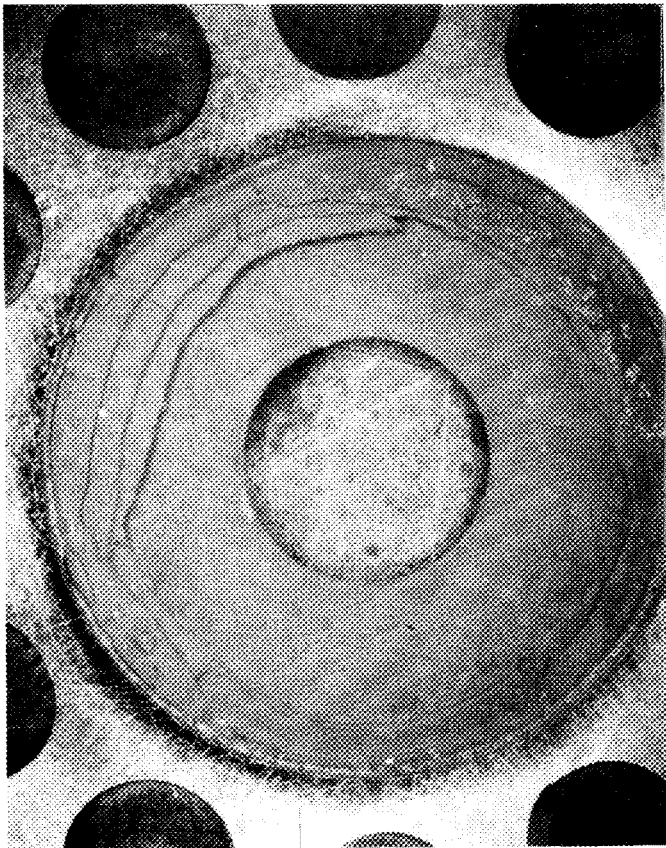
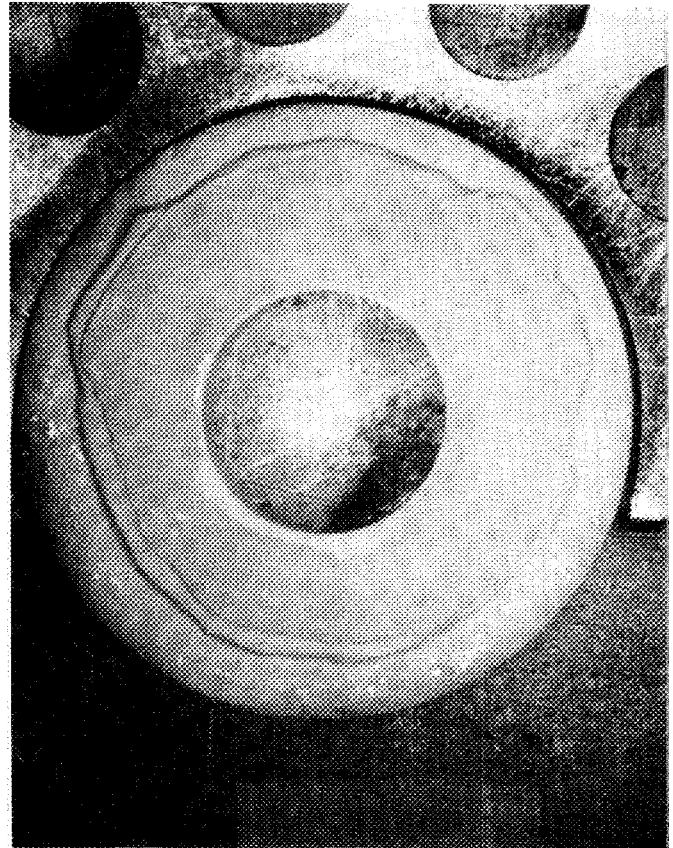
The brazed assemblies were also subjected to thermal cycling on a schedule similar to that which would be required of each subassembly during subsequent brazes of the final anode assembly. The subassemblies were placed in a molybdenum boat, fired in dry hydrogen at 1010°C for 10 minutes and allowed to cool to room temperature. This cycle was repeated twice before peel testing.

Six samples were brazed and tested. The results are given in Table I.

From the six tests, one joint made using ductile braze alloy (Sample 3) demonstrated the highest peel strength even after thermal cycling. However, samples 5 and 6 showed substantially lower peel strengths. The brittle braze alloy joint (Sample 4) also showed a high bond strength because the break in this sample did not occur in the interface, but in the silicon carbide loaded beryllia. Also indicated by the nature of the break (Figure 6) is that the failure is caused by the thermal expansion differences between the materials. The poor bond strengths of samples 1 and 2 are due to insufficient braze alloy at the interfaces.

Although the number of samples was inadequate to obtain statistically valid measurements of braze joint properties, the qualitative evidence favors the use of the ductile braze joint in the anode subassemblies.

Cracked Silicon Carbide Loaded
Beryllia Piece on Copper Ring



Copper Ring with Pieces of Silicon Carbide
Loaded Beryllia Attached

FIGURE 6. CRACKED SURFACES AFTER THERMAL CYCLING

Table I
Peel Tests

SAMPLE #	BRAZE JOINT	PEEL STRENGTH (lb/in)	REMARKS
1	Brittle	43	No thermal cycle.
2	Brittle	---	Top copper piece fell off of silicon carbide loaded beryllia ring during thermal cycle. Insufficient braze alloy.
3	Ductile	166	After three thermal cycles at 1010°C.
4	Brittle	(1) 114 (2) ---	Two tests were performed (1) Peel test before thermal cycle. (2) The remaining parts of the sample were thermal cycled at 1010°C three times. No peel test was done because the joint failed under the radial shear caused by thermal expansion mismatch between the two materials.
5	Ductile	32	No thermal cycle.
6	Ductile	43	After thermal cycle at 1010°C.

VI. COLLECTOR

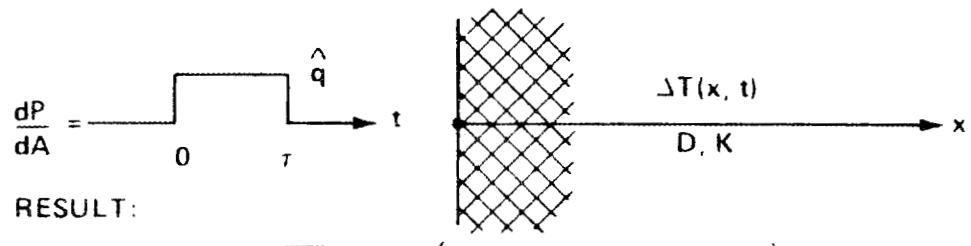
The problem of transient heating in the gyrotron collector, to determine the effect of hydrodynamic and geometric parameters on heat transport in the long pulse regime, is being analyzed. As a first step in the analysis, one dimensional transient heat transport calculations have been made. Further work on this topic is planned with two dimensional modeling and will be carried out with the aid of a transient heat transport code.

The one dimensional transient heat transport analysis is based on "initial value" calculations and the results are therefore valid only for a single heat flux pulse of amplitude \hat{q} (watts/cm²) and duration τ (sec). In practice, of course, all pulsed devices will be required to withstand finite duty, $v \equiv \tau/\Delta$ where Δ is the pulse repetition period. For very low duties, the single pulse analysis is valid, but for $v \geq 0.02$ one must consider the presence of the residual temperature profile which results from an infinite pulse train.

The single heat impulse is turned on at the collector wall at time $t = 0$ and terminated at $t = \tau$. For very short times, the heat pulse will not penetrate through the collector wall material to the cooling channels. The collector wall then appears to be semi-infinite as shown in Figure 7. The one dimensional heat diffusion equation

$$\frac{\partial^2 \Delta T(x,t)}{\partial x^2} - \frac{1}{D} \frac{\partial \Delta T(x,t)}{\partial t} = 0 \quad (1)$$

for the temperature rise, $\Delta T(x,t)$, above the ambient (coolant) temperature, T_c , has been solved. The parameter D is the thermal diffusivity of the collector wall material. The boundary conditions for the semi-infinite slab model are



RESULT:

FIGURE 7: INFINITELY THICK SLAB

$$\frac{\partial \Delta T (o,t)}{\partial X} = \frac{-q (o,t)}{K} \quad (2)$$

$$\text{with } q(o,t) = \begin{cases} \hat{q} & 0 < t < \tau \\ 0 & t > \tau \end{cases}$$

and

$$\Delta T (\infty,t) = 0 \quad (3)$$

The solution is ¹⁰

$$\begin{aligned} \Delta T(x,t) &= \frac{2\hat{q}\sqrt{D}}{\sqrt{\pi} K} \left[\sqrt{t} \left\{ 2\sqrt{\frac{3}{2}} \operatorname{ierfc} \left(\frac{x}{2\sqrt{Dt}} \right) \right\} \right]_{0 < t < \tau} \\ &= \frac{2\hat{q}\sqrt{D}}{\sqrt{\pi} K} \left[\sqrt{t} \left\{ 2\sqrt{\frac{3}{2}} \operatorname{ierfc} \left(\frac{x}{2\sqrt{Dt}} \right) \right\} \right. \\ &\quad \left. - \sqrt{t-\tau} \left\{ 2\sqrt{\frac{3}{2}} \operatorname{ierfc} \left(\frac{x}{2\sqrt{D(t-\tau)}} \right) \right\} \right]_{t > \tau} \end{aligned} \quad (4)$$

If we set $x = 0$ in (4) we find that the quantities in the curly brackets go to unity. The peak temperature rise at the collector wall is then

$$\Delta T(x=0) \Big|_{\max} = \frac{2\hat{q}\sqrt{D\tau}}{\sqrt{\pi} K} \quad (5)$$

For copper, with an incident heat flux of 1 kW/cm^2 (5) becomes

$$\Delta T(x=0) \Big|_{\max} (\text{°C}) = 299 \sqrt{\tau(\text{sec})} \quad (6)$$

By inspection of (4) we see that the heat pulse penetrates the collector wall a distance $\hat{L} \sim 2\sqrt{Dt}$. If the water channels are located a distance L from the collector wall, then the heat pulse will reach the water channel in a time $\hat{t} \sim L^2/4D$. For our present pulsed collector design, this time is on the order of 50-100 msec. Therefore, for a pulse duration in excess of 50 msec the analysis must be generalized to consider the heat transfer into the coolant. The generalized one dimensional geometric model is shown in

Figure 8. The heat diffusion equation (1) must now be solved subject to a new set of boundary conditions:

$$\frac{\partial \Delta T(0,t)}{\partial x} = \frac{-q(0,t)}{K}, \text{ as before} \quad (7)$$

while

$$\frac{\partial \Delta T(L,t)}{\partial x} = - \frac{h(t)\Delta T(L,t)}{K} \quad (8)$$

where $h(t)$ is the heat transfer coefficient of the water channel boundary layer. By invoking (8), we assume that the water channel boundary layer a) has zero heat capacity b) is spatially much thinner than the wall thickness, L , and c) supports heat flow which may always be considered steady state compared to the other thermal time scales in the problem.

The heat transfer coefficient h is in general a complicated function of the hydrodynamic parameters as well as the absolute temperature T of the water channel wall. Qualitatively, h is roughly independent of T in the "convection cooling" regime ($T \lesssim 100^\circ\text{C}$). Once the water channel wall temperature exceeds the boiling point, the boundary layer supports the formation of small bubbles which are continuously reabsorbed in the bulk of the coolant. This regime of operation "nucleate boiling", provides greatly improved heat transport, and the heat transfer coefficient is a strongly increasing function of T until the burnout condition occurs¹¹. At this point the turbulent fluid boundary layer is replaced by a blanket of superheated steam and the heat transfer coefficient drops radically.

As long as the water channel wall temperature does not exceed 100°C , we may approximate $h(t) = h = \text{constant}$. Then for $t < \tau$ equation (1) can be solved subject to (7) and (8)¹².

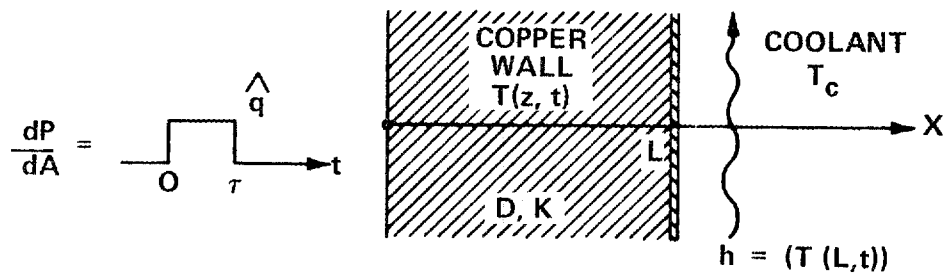


FIGURE 8. SLAB OF FINITE THICKNESS

$$\Delta T(x,t) = \frac{\hat{q} L}{K} \left[\frac{1}{B} + \left(1 - \frac{x}{L}\right) - 2 \sum_i \frac{e^{-Dy_i^2 t/L^2} \left(\cos \frac{y_i x}{L} \right) \left[y_i^2 + B^2 \right]}{y_i^2 \left[y_i^2 + B^2 + B \right]} \right] \quad (9)$$

$0 < t < \tau$

where $B \equiv h L/K$ is the thermal conductance of the water channel boundary layer normalized to the thermal conductance of the collector wall, and the y_i 's are the positive roots of

$$\cot y = \frac{y}{B} \quad (10)$$

The sum \sum_i in (9) represents a spectrum of highly damped "heat waves" with "wavenumbers" which are "resonant" according to (10). The first three roots of (10) are plotted in Figure 9 versus the thermal conductance parameter B . Typically, only the first and possibly the second roots of (10) are required for appropriate convergence of the sum \sum_i in (9). For times $t > \tau$, we may apply Duhamel's theorem to (9) and we obtain

$$\Delta T(x,t) = \frac{\hat{q} L}{K} \sum_i \frac{\left(\cos \frac{y_i x}{L} \right) \left[y_i^2 + B^2 \right]}{y_i^2 \left[y_i^2 + B^2 + B \right]} \left\{ e^{-Dy_i^2 (t-\tau)/L^2} - e^{-Dy_i^2 t/L^2} \right\} \quad (11)$$

$t > \tau$

We have used equations (9) and (11) to calculate the transient temperature profiles for a case of particular interest for the 60 GHz 100 msec pulsed tube (Table II).

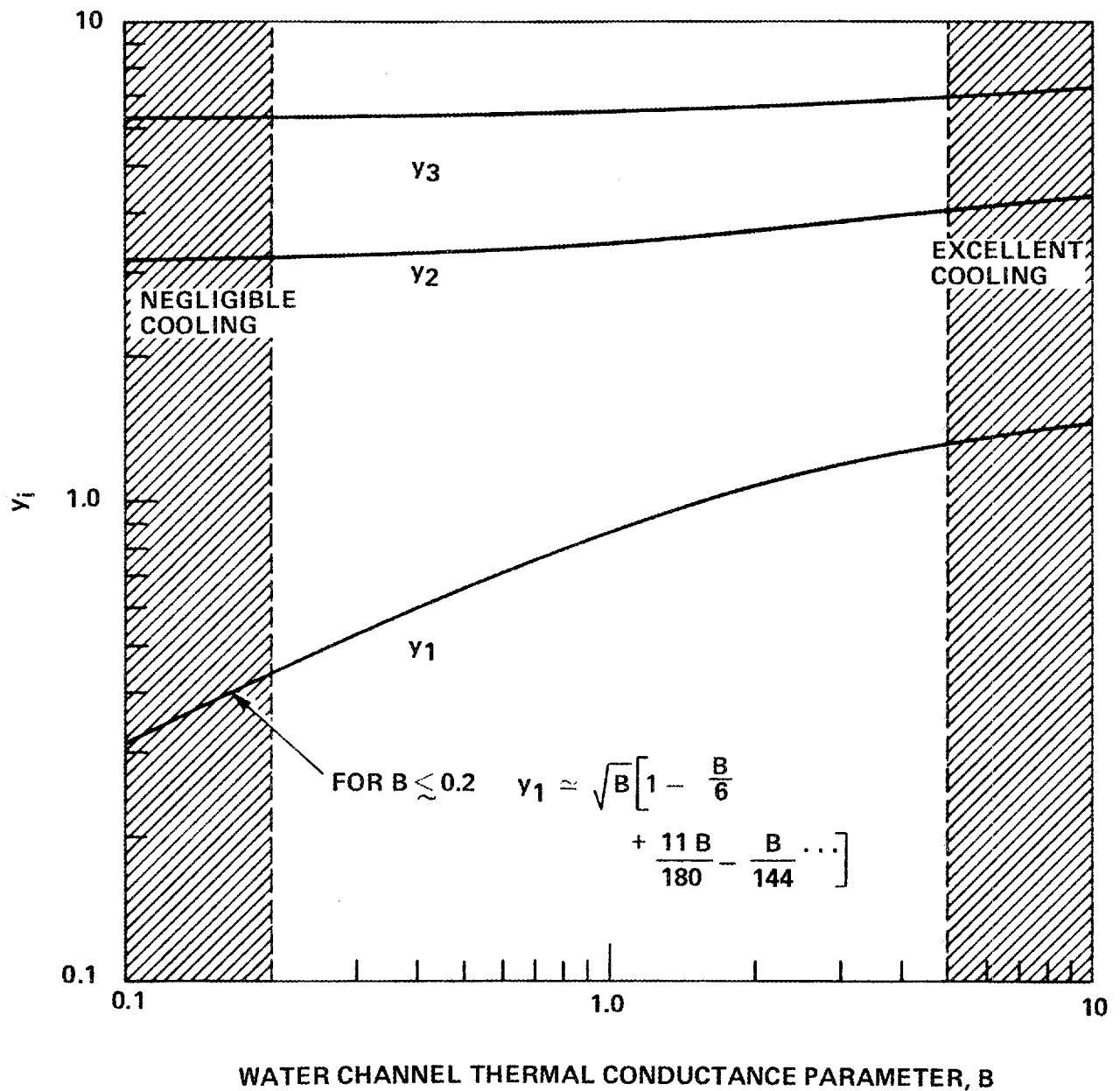


FIGURE 9. ROOTS OF $\cot y = \frac{y}{B}$

Table II
Parameters for Cooling Calculations (Figure 10)

coolant temperature	35°C
coolant pressure	100 psig
coolant velocity	0.91 ft/sec
coolant flow	2 gpm
coolant heat transfer coefficient	0.22 watts/cm ² -°C
incident heat flux	1 kW/cm ²
wall thickness	0.508 cm
wall thermal conductivity	4.0 watts/cm-°C
wall thermal diffusivity	1.12 cm ² /sec
pulse length	100 msec
duty	10 ⁻³

The cooling parameters in Table II were chosen to provide sufficient cooling for the average power (1 watt/cm²). The resulting time history for the temperature profile (Figure 10) shows that the cooling parameters are indeed sufficient to hold temperature excursions within the design limits. Note that the thermal conductance of the water channel for this case is very low compared to that of the copper wall; the water channel boundary acts like an insulator during the heat pulse. The assumption, $h = \text{constant}$, which was used in calculating these profiles is (in hindsight) valid because the water channel wall temperature never exceeds the point of transition (~ 100°C) from convection cooling to nucleate boiling. On a timescale large compared to the pulse length, the temperature profile labeled as "200 msec" decays uniformly to the coolant temperature in a time $\sim LK/hD \sim 10$ seconds. Thus the peak bulk water temperature excursion is $\sim 25^\circ\text{C}$ while the average, bulk water temperature excursion is $\sim 2.5^\circ\text{C}$.

From the temperature profiles shown in Figure 10, we expect that for the cooling parameters in Table II and pulse lengths on the order of several hundred milliseconds, the temperature excursion at the water channel wall will not exceed the burnout temperature. However, detailed two dimensional transient heat transport calculations must be performed before the rated pulse length of the 60 GHz pulsed tube may be extended beyond 100 msec. The

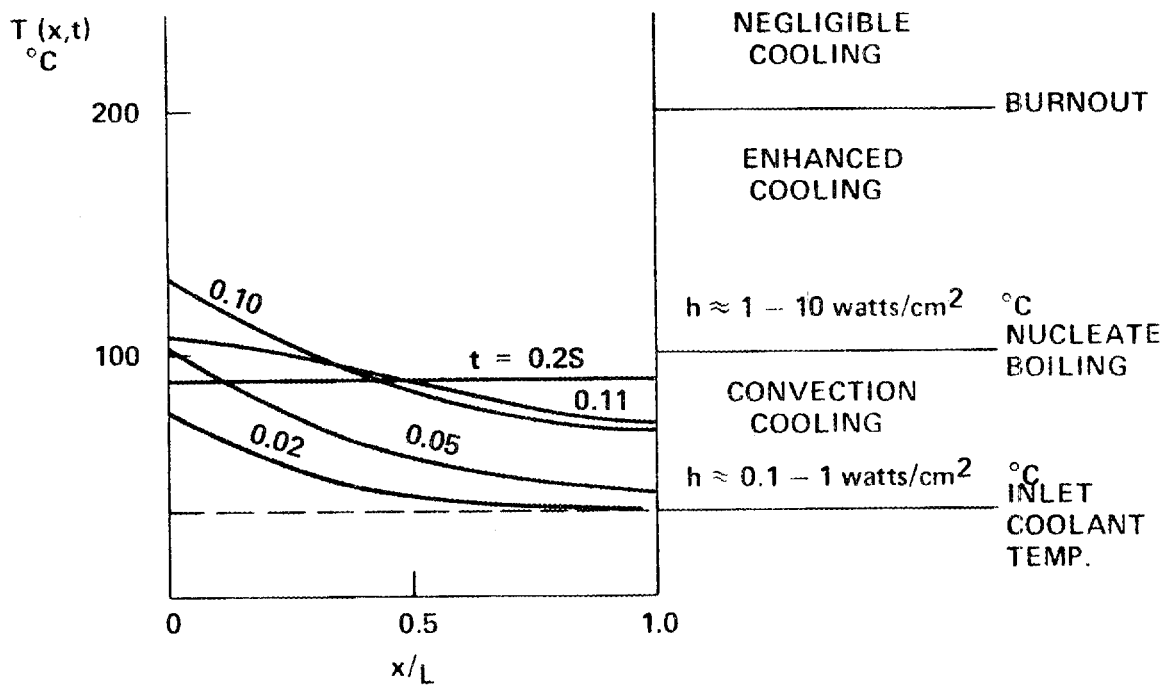


FIGURE 10. TRANSIENT TEMPERATURE PROFILES IN COLLECTOR WALL

conclusions of the one dimensional collector calculations are summarized in Figure 11.

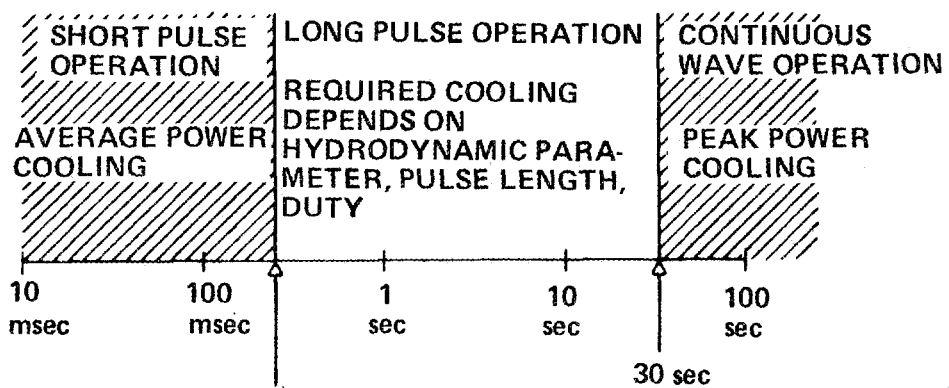


FIGURE 11. PULSE DURATION REGIMES FOR GYROTRON COLLECTORS

VII. WINDOW

Further cold testing of 60 GHz single disc BeO windows was undertaken this quarter. Window discs were cold tested using two different techniques as shown in Figure 12. A conventional measurement of the standing wave ratio of the window discs was performed using the set-up shown in Figure 12a. A transducer (TRG model #V330) was used to launch a TE_{01}^o wave toward the window and the standing wave ratio was measured with a slotted line in the TE_{10} portion of the transmission line. This technique suffers from several disadvantages. First, circular electric mode transducers are characteristically narrow band and poorly matched, even at their center frequency; this prevents making an accurate broadband measurement of window VSWR. Second, the actual mode of interest for the window cold test is the TE_{02}^o mode. The match of the window for the TE_{02}^o mode must be simulated measuring VSWR versus frequency for the TE_{01}^o mode and then scaling the abscissa of the resulting VSWR curve by the ratio of the guide wavelengths for the TE_{01}^o and the TE_{02}^o modes.

The cold test arrangement shown in Figure 12b has also been used to study the window match. For this set-up, a cold test model of the actual 60 GHz tube was built to simulate the rf properties of the region from the cavity to the end of the collector. This structure was terminated with various window discs and the effect on the cavity resonance curve was observed. The thickness of each window disc was adjusted until the window mismatch did not cause an appreciable change in the loaded cavity Q. We found that for the discs of $3/2$ thickness employed on this tube, the disc thickness necessary to provide an acceptable match is critical. This follows from the fact that the bandwidth for a $3/2$ window is only a few times larger than the cavity resonance bandwidth.

We have developed a procedure for fabricating single disc window assemblies which ensures that the proper disc thickness is achieved. The unmetallized discs are fabricated to the specification shown in Figure 13. Note that the tolerances on parallelism and flatness are stringent. The former is required to maintain a uniform reflection coefficient across the window face while the latter is needed to allow subsequent grinding

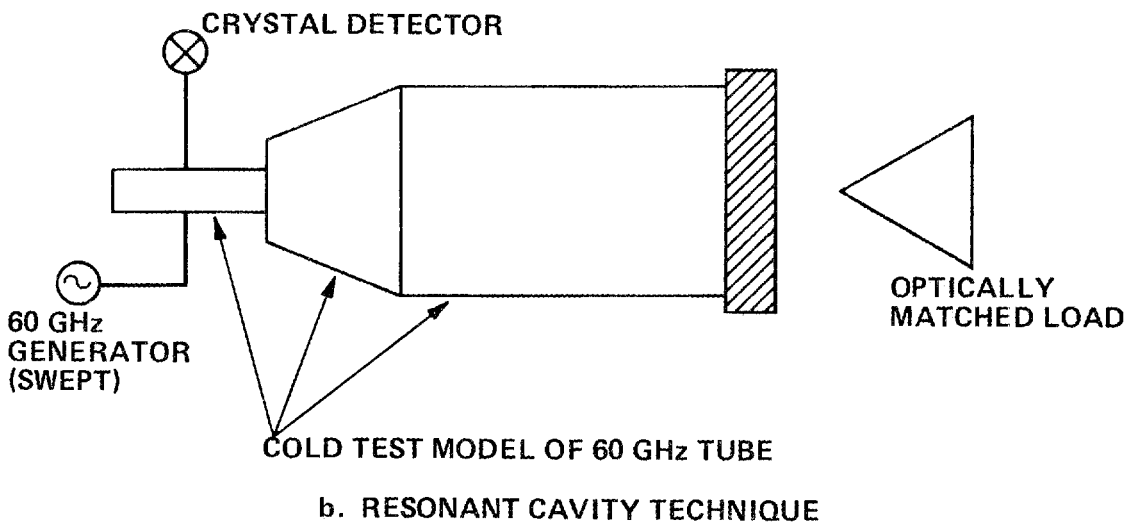
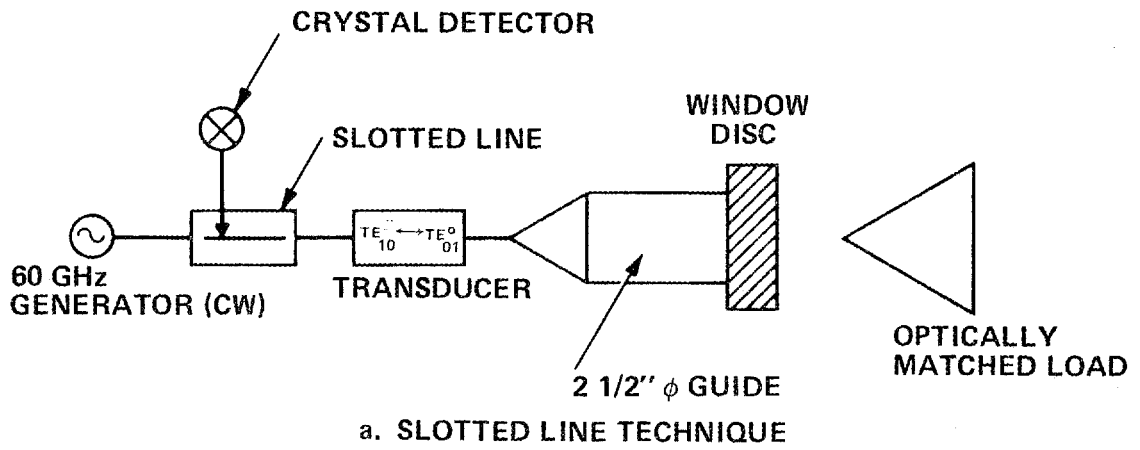


FIGURE 12. WINDOW COLD TEST ARRANGEMENTS

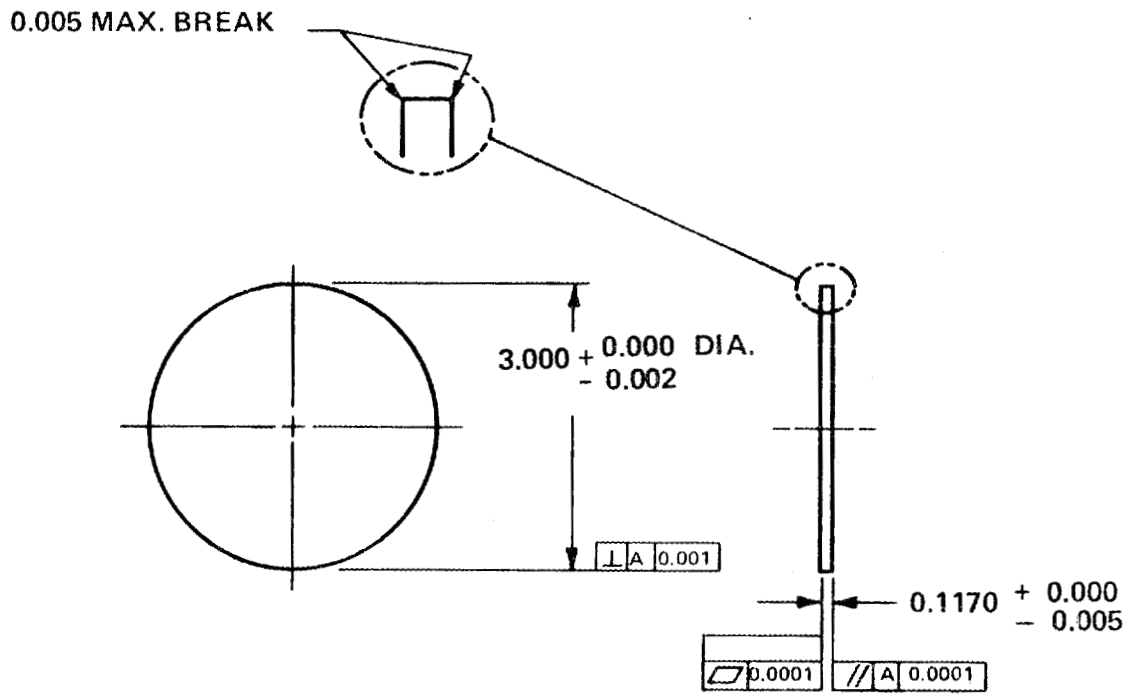


FIGURE 13. CERAMIC DISC

operations which can maintain the requisite parallelism. After the mismatches of the unmetallized discs are measured, each individual disc is ground down by an appropriate amount and cold tested again. This process is repeated as necessary until each disc is matched. The discs are then metallized and brazed into the window assembly. Although sufficient experience with the cold test techniques to claim accurate statistical results on the homogeneity of the BeO ceramics has not yet been acquired, it appears that within a single batch there may be a variation in dielectric constant of $\sim 0.5\%$ while an $\sim 1.0\%$ variation from batch to batch may be observed.

VIII. COMPONENTS

A variety of waveguide components is being developed for use with the 60 GHz gyrotron including waterloads, a frequency sampler and arc detector, mode filters, miter bends and adapters.

A. WATERLOADS

A pulsed waterload has been designed. The outline of the pulsed waterload is shown in Figure 14. The first waterload is being assembled and will be completed in time for use in testing the first experimental tube.

A CW waterload is being designed.

B. FREQUENCY SAMPLER AND ARC DETECTOR

A frequency sampler and arc detector has been designed. The outline is shown in Figure 15. The arc detector includes a test lamp for checking the arc detector system. The unit also includes a gas port for introducing dry nitrogen into the waveguide section for applications located in humid climates.

C. MODE FILTERS

Two types of mode filters are being designed. The first type is a water cooled stainless steel waveguide, which utilizes the differential in loss between non-circular electric modes and circular electric modes. The second type of mode filter consists of alternating stainless steel rings and gaps backed up by a waterloaded ceramic cylinder. In addition to the mode filtering mechanism of the first type of mode filter, the second type creates breaks in the conducting wall for non-circular electric modes but not for circular electric modes.

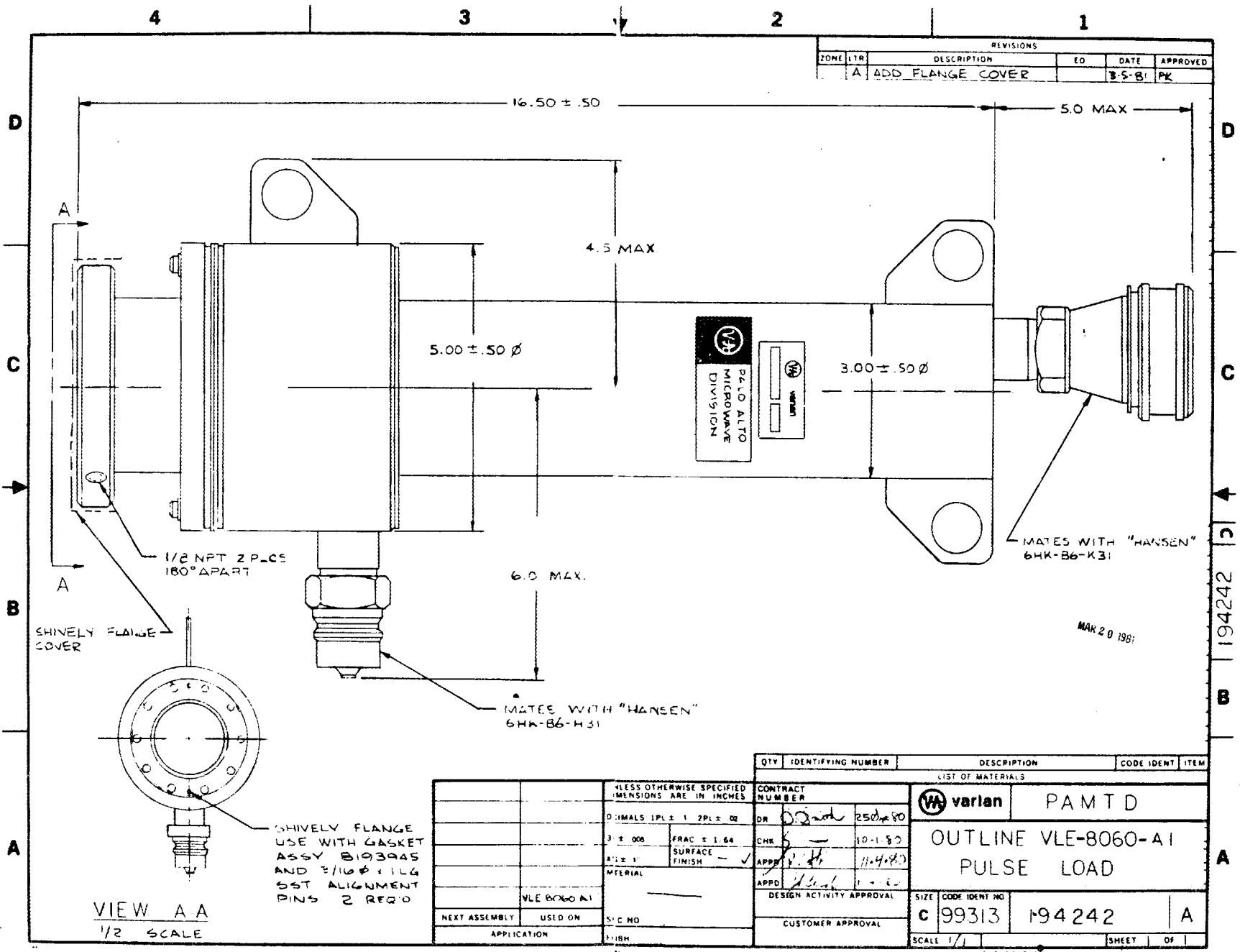
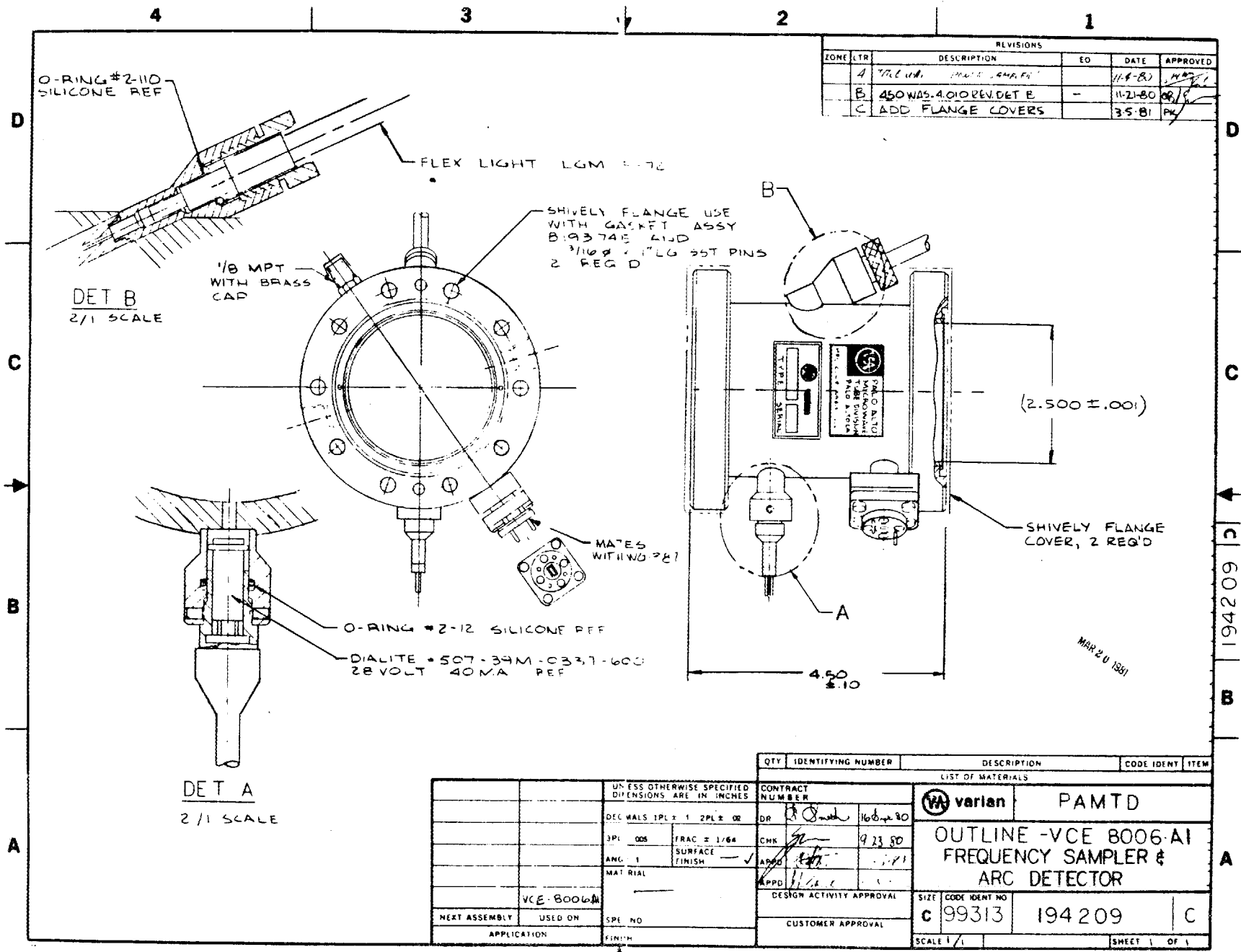


FIGURE 14. PULSED WATERLOAD



REVISIONS					
ZONE	LTR	DESCRIPTION	EO	DATE	APPROVED
A		TITLE CHG. FROM 8006-A1		11-8-80	MAR
B		450 WAS 4010 REN DET E	-	11-21-80	OR/S
C		ADD FLANGE COVERS		3-5-81	PK

QTY	IDENTIFYING NUMBER	DESCRIPTION	CODE IDENT	ITEM
LIST OF MATERIALS				
		varian	PAMTD	
		OUTLINE -VCE 8006-A1		
		FREQUENCY SAMPLER &		
		ARC DETECTOR		
DESIGN ACTIVITY APPROVAL		SIZE	CODE IDENT NO	
CUSTOMER APPROVAL		C	99313	194209
SCALE 1/1		SHEET 1 OF 1		

FIGURE 15. OUTLINE VCE-8006-A1 FREQUENCY

D. MITER BEND

A mitered 90° circular waveguide bend is being designed for potential waveguide configuration tests.

E. FLANGE ADAPTERS

Flange adapters to adapt from the copper gasketed flange to both the male and female 28 GHz flange designs are being designed. This will allow use of certain waveguide component designs developed on the 28 GHz program.

IX. TUBE ASSEMBLY

A. VGE-8060X1

The first experimental pulsed 60 GHz gyrotron is ready for the pump. Evacuation and bakeout will commence January 6.

B. VGE-8060S1

Assembly of the first 100 ms pulse duration gyrotron has started. The collector sump assemblies, the tubulation assembly, the output taper assembly, the body cylinder assembly, one collector seal assembly and the anode first braze assembly are complete.

C. VGE-8060S2

Assembly of the second 100 ms pulse duration gyrotron has started. The top collector sump assembly and the body cylinder assembly are complete.

X. PROGRAM SCHEDULE AND PLANS

The first experimental pulsed 60 GHz gyrotron is ready for the pump. Evacuation and bakeout will commence January 6. Testing of this build will be completed during the next quarter. Final assembly of the first 100 ms pulse duration gyrotron will be delayed until some test data are obtained from the experimental tube.

Procurement of the spare solenoid magnet will be delayed until some operation with the experimental tube has been experienced. An order will be placed around the first of April.

Assembly of the frequency sampler and arc detector and pulsed waterload will be complete in time for testing the experimental tube.

Assembly of major subassemblies for the second 100 ms pulse duration gyrotron were started this quarter and will continue next quarter.

Assembly drawings for the major subassemblies for the first 30 s pulse duration gyrotron will be completed next quarter.

The short pulse test set modification was completed on a separate contract this quarter. A certain amount of debugging is anticipated in conjunction with experimental tube testing early next quarter. Long pulse test set modification will start next quarter after experimental tube test.

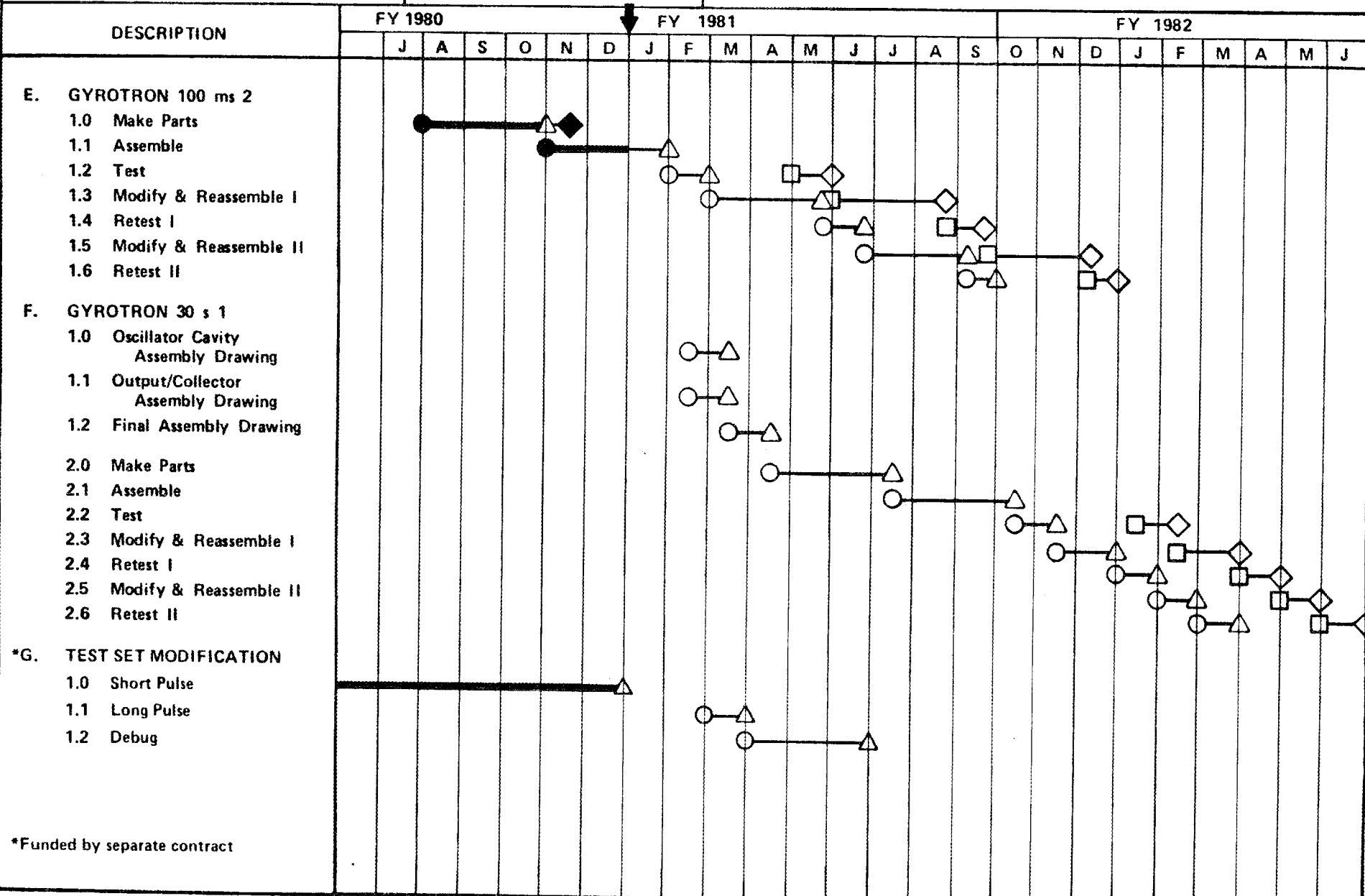
Several areas of gyrotron behavior were investigated during the quarter. An arcing and crowbar investigation was begun using available gyrotrons. The computer investigation of voltage gradients and trapped electrons was completed. RF behavior was studied using VGA-8000 S/Ns 8 and 11.

The milestone chart and status report is shown in Figure 16.

MILESTONE CHART AND STATUS REPORT

○ ORIGINAL START □ REVISED START △ MAJOR MILESTONE
 ▽ INTERMEDIATE OR DECISION POINT ◇ PROPOSED SCHEDULED DEVIATION FOR A MAJOR MILESTONE
 ↓ STATUS REPORT TIME — ACTIVITY SCHEDULED — ACTIVITY COMPLETED

PROGRAM: 60 GHz DEVELOPMENT JOB NO.: STATUS REPORT DATE: DECEMBER 1980



*Funded by separate contract

39

MILESTONE CHART AND STATUS REPORT

○ ORIGINAL START □ REVISED START △ MAJOR MILESTONE
 ▽ INTERMEDIATE OR DECISION POINT ◇ PROPOSED SCHEDULED DEVIATION FOR A MAJOR MILESTONE
 ↓ STATUS REPORT TIME — ACTIVITY SCHEDULED — ACTIVITY COMPLETED

PROGRAM
60 GHz DEVELOPMENT

JOB NO.

STATUS REPORT DATE
DECEMBER 1980

DESCRIPTION	FY 1981							FY 1982											FY 1983						
	A	M	J	J	A	S	O	N	D	J	F	M	A	M	J	J	A	S	O	N	D	J	F	M	
H. GYROTRON 30 s 2																									
1.0 Make Parts																									
1.1 Assemble																									
1.2 Test																									
1.3 Modify & Reassemble I																									
1.4 Retest I																									
1.5 Modify & Reassemble II																									
1.6 Retest II																									
I. GYROTRON CW 1																									
1.0 Make Parts																									
1.1 Assemble																									
1.2 Test																									
1.3 Modify & Reassemble I																									
1.4 Retest I																									
1.5 Modify & Reassemble II																									
1.6 Retest II																									
1.7 Ship																									
J. 60 GHz COMPONENTS																									
1.0 Build CW Load																									
2.0 Build Deliverable Power Sampler Arc Detector																									
3.0 Build Deliverable CW Load																									

40

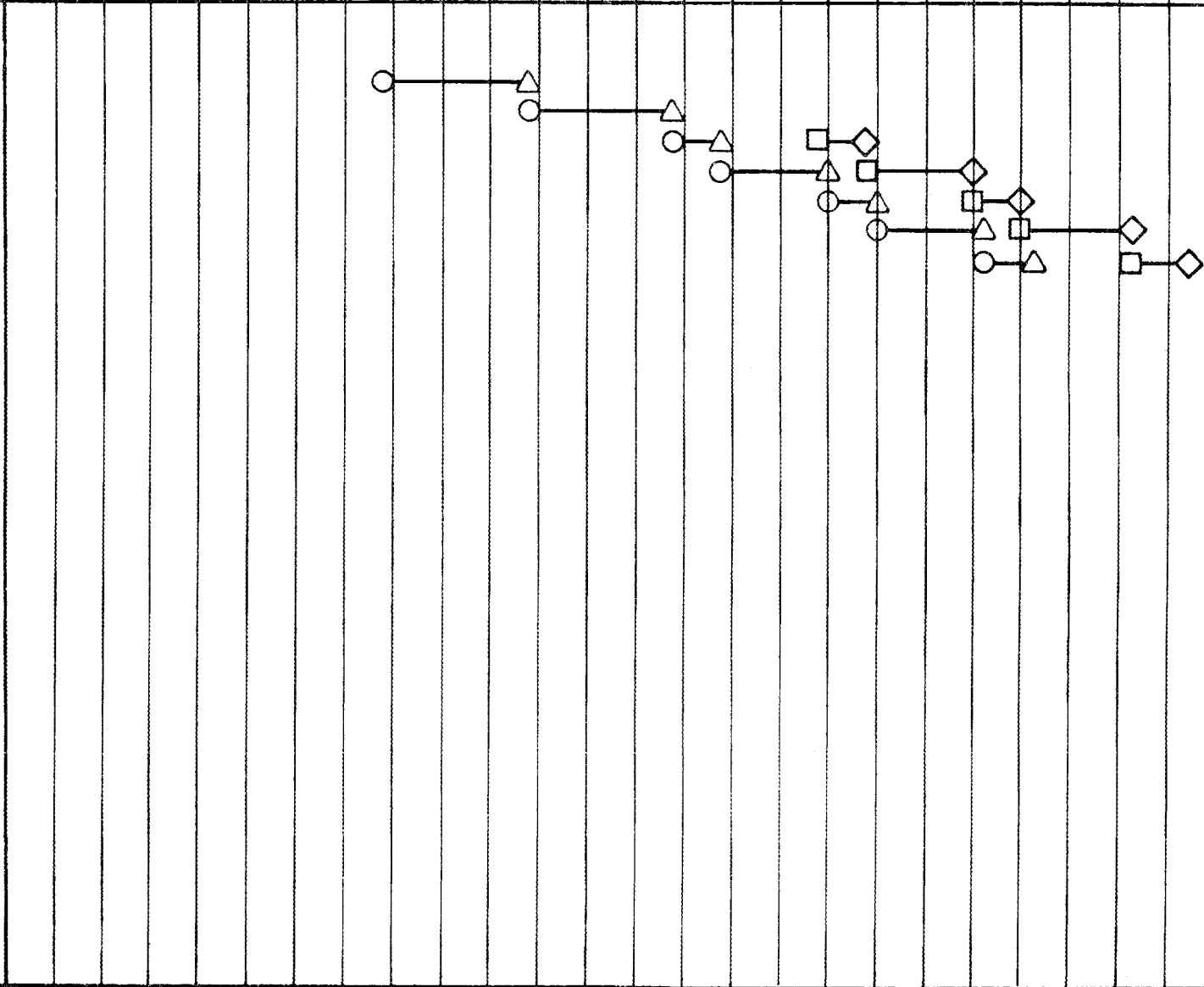
MILESTONE CHART AND STATUS REPORT

○ ORIGINAL START □ REVISED START △ MAJOR MILESTONE
 ▽ INTERMEDIATE OR DECISION POINT ◇ PROPOSED SCHEDULED DEVIATION FOR A MAJOR MILESTONE
 ↓ STATUS REPORT TIME — ACTIVITY SCHEDULED — ACTIVITY COMPLETED

PROGRAM: 60 GHz DEVELOPMENT JOB NO.: STATUS REPORT DATE: DECEMBER 1980

DESCRIPTION FY 1982 (D, J, F, M, A, M, J, J, A, S) FY 1983 (O, N, D, J, F, M, A, M, J, J, A, S) FY 1984 (O, N, D)

- K. GYROTRON CW 2
- 1.0 Make Parts
- 1.1 Assemble
- 1.2 Test
- 1.3 Modify & Reassemble I
- 1.4 Retest I
- 1.5 Modify & Reassemble II
- 1.6 Retest II
- 1.7 Ship



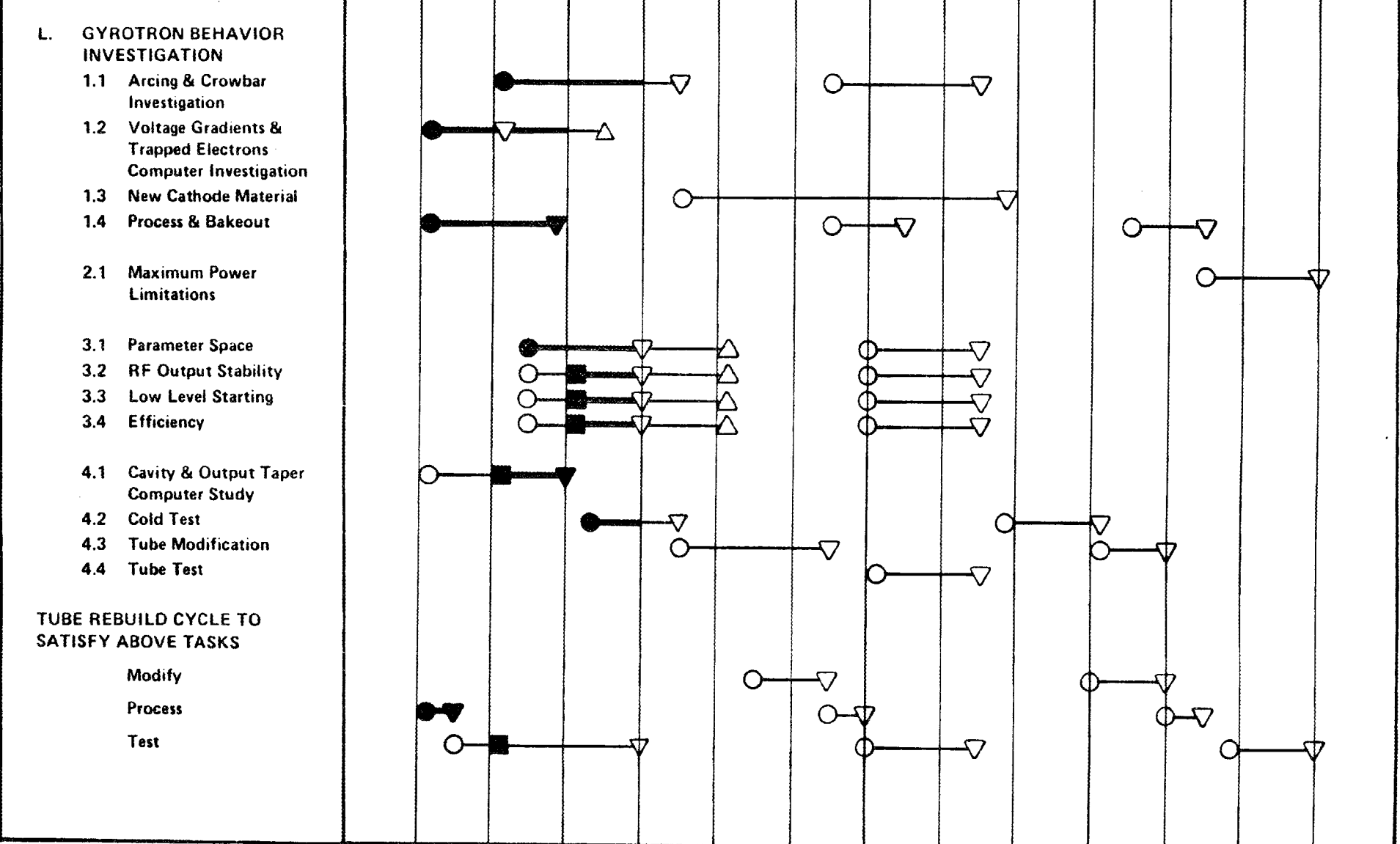
MILESTONE CHART AND STATUS REPORT

○ ORIGINAL START □ REVISED START △ MAJOR MILESTONE
 ▽ INTERMEDIATE OR DECISION POINT ◇ PROPOSED SCHEDULED DEVIATION FOR A MAJOR MILESTONE
 ↓ STATUS REPORT TIME — ACTIVITY SCHEDULED — ACTIVITY COMPLETED

PROGRAM: 60 GHz DEVELOPMENT JOB NO.: STATUS REPORT DATE: DECEMBER 1980

DESCRIPTION: FY 1981

42



XI. REFERENCES

1. H.R. Jory, E.L. Lien, and R.S. Symons, Final Report, "Millimeter Wave Study Program", Oak Ridge National Laboratory Order No. Y12 11Y-49438 V, Varian Associates, Inc., November 1975.
2. D.V. Kisel, G.S. Korablev, V. G. Navel'yev, M.I. Petelin and Sh. E. Tsimring, "An Experimental Study of a Gyrotron, Operating at the Second Harmonic of the Cyclotron Frequency, with Optimized Distribution of the High Frequency Field," Radio Engineering and Electronic Physics, Vol. 19, No. 4, 95-100, 1974.
3. S. Hegji, H. Jory and J. Shively, "Development Program for a 200 kW CW, 28 GHz Gyroklystron" Quarterly Report No. 6, Union Carbide Corporation Contract No. 53X01617C, Varian Associates, Inc., July through September 1977.
4. H. Jory, S. Evans, S. Hegji, J. Shively, R. Symons and N. Taylor "Development Program for a 200 kW, CW 28 GHz Gyroklystron", Quarterly Report No. 9, Union Carbide Corporation Contract No. W-7405-eng-26, ORNL Sub-01617/9, Varian Associates, Inc., April through June 1978.
5. V.A. Flyagin, et al, "The Gyrotron", IEEE Trans. MTT-25, No. 6 pp. 522-527, June 1977.
6. J.F. Shively et al, "Recent Advances in Gyrotrons," 1980 IEEE MTT-S International Microwave Symposium Digest, 28-30 May 1980, Washington, D.C. IEEE Catalog No. 80CH1545-3 MTT, pp 99-101.
7. F. Friedlander, E. Galli, H. Jory, F. Kinney, K. Miller, J. Shively and R. Symons, "Development Program for a 200 kW, CW, 28 GHz Gyroklystron", Quarterly Report No. 1, Union Carbide Corporation Contract No. 53X01617C, Varian Associates, Inc., October 1976.
8. F. Friedlander, E. Galli, H. Jory, K. Miller, J. Shively, and R. Symons, "Development Program for a 200 kW, CW 28 GHz Gyroklystron," Quarterly Report No. 2, Union Carbide Corporation Contract No. 53X01617C, Varian Associates, Inc. October 1976.
9. See for example, G.B. Collins, Microwave Magnetrons, M.I.T. Radiation Laboratory Series, 6 McGraw-Hill, New York 1948, p. 520.
10. Carslaw and Jaeger, Conduction of Heat in Solids, Oxford Press, London 1959
11. W.H. McAdams, Heat Transmission, McGraw-Hill, New York 1954, p. 389, S.Mirshak, W.S. Durant and R.H. Towell, "Heat Flux at Burnout", E.I. duPont de Nemours and Co., AEC Research and Development Report, February 1959.
12. M.L. Anthony, "Temperature Distributions in Composite Slabs due to a Suddenly Activated Plane Heat Source", Instn. Mech. Engrs., London and ASME, New York, 1951 pp 236-249.

INTERNAL DISTRIBUTION

- | | |
|-----------------------|--|
| 1. A. L. Boch | 15. T. L. White |
| 2. J. L. Burke | 16-17. Laboratory Records Department |
| 3. R. J. Colchin | 18. Laboratory Records, ORNL-RC |
| 4-7. H. O. Eason | 19. Y-12 Document Reference Section |
| 8. O. C. Eldridge | 20-21. Central Research Library |
| 9. R. P. Jernigan | 22. Fusion Energy Division Library |
| 10-12. C. M. Loring | 23. Fusion Energy Division Communications Center |
| 13. H. C. McCurdy | 24. ORNL Patent Office |
| 14. D. B. Morgan, Jr. | |

EXTERNAL DISTRIBUTION

25. R. A. Dandl, 1122 Calle De Los Serranos, San Marcos, CA 92069
26. R. J. DeBellis, McDonnell Douglas Astronautics Co., P.O. Box 516, St. Louis, MO 63166
27. A. N. Dellis, Culham Laboratory, Abingdon, Oxon, England, OX1430B
28. W. P. Ernst, Princeton University, Plasma Physics Laboratory, P.O. Box 451, Princeton, NJ 08540
29. W. Friz, AFAL/DHM, Wright Patterson AFB, OH 45433
30. T. Godlove, Particle Beam Program, Office of Inertial Fusion, Department of Energy, Mail Stop C-404, Washington, DC 20545
31. V. L. Granatstein, Naval Research Laboratory, Code 6740, Washington, DC 20375
32. G. M. Haas, Component Development Branch, Office of Fusion Energy (ETM), Department of Energy, Mail Stop G-234, Washington, DC 20545
33. J. L. Mirshfield, Yale University, Department of Engineering and Applied Science, P.O. Box 2159, Yale Station, New Haven, CT 06520
34. H. Ikegami, Institute of Plasma Physics, Nagoya University, Nagoya 464, Japan
35. J. V. Lebacqz, Stanford Linear Accelerator Center, P.O. Box 4349, Stanford, CA 94305
36. W. Lindquist, Electronics Engineering Department, Lawrence Livermore Laboratory, P.O. Box 808/L-443, Livermore, CA 94550
37. K. G. Moses, TRW Defense & Space Systems, 1 Space Park, Bldg. R-1, Redondo Beach, CA 90278
38. M. R. Murphy, Office of Fusion Energy (ETM), Department of Energy, Mail Stop G-234, Washington, DC 20545
39. V. B. Mapper, Three Dunwoody Park, Suite 112, Atlanta, GA 30341
40. G. F. Pierce, 53 Lomond Drive, Inverness, IL 60067
41. B. H. Quon, TRW Defense & Space Systems, 1 Space Park, Bldg. R-1, Redondo Beach, CA 90278
42. M. E. Read, Naval Research Laboratory, Code 6740, Washington, DC 20375
43. D. B. Reimsen, General Atomic Company, P.O. Box 81608, San Diego, CA 92138
44. G. Simons, Harry Diamond Laboratory, 2800 Powder Mill Road, Adelphi, MD 20783
45. B. Stallard, Lawrence Livermore Laboratory, University of California, L-437, P.O. Box 806, Livermore, CA 94550
46. H. S. Staten, Office of Fusion Energy (ETM), Department of Energy, Mail Stop G-234, Washington, DC 20545
47. P. Tallierico, AT-1, Accelerator Technology Division, Los Alamos Scientific Laboratory, Mail Stop 817, P.O. Box 1663, Los Alamos, NM 87545

ORNL/SUB-79/21453/
January 30, 1981

48. J. J. Tancredi, Hughes Aircraft Company, Electron Dynamics Division, 3100 W. Lomita Blvd., Torrance, CA 90509
49. R. J. Temkin, National Magnet Laboratory, Massachusetts Institute of Technology, Cambridge, MA 02139
50. A. Trivelpiece, Science Applications, Inc., 1200 Prospect Street, P.O. Box 2351, LaJolla, CA 92038
51. Director, U.S. Army Ballistic Missile Defense Advance Technology Center, Attn.: D. Schenk, ATC-R, P.O. Box 1500, Huntsville, AL 35807
- 52-53. Department of Energy Technical Information Center, Oak Ridge, TN 37830
54. RADC/OCTP, Griffiss AFB, NY 13441
55. Office of Assistant Manager for Energy Research and Development, Oak Ridge Operations Office, Department of Energy, Oak Ridge, TN 37830

VARIAN DISTRIBUTION

- 56. R. Berry
- 57. M.K.Cheng
- 58. S. Evans
- 59. S. Evers
- 60. K. Felch
- 61. P. Ferguson
- 62. T.J. Grant
- 63. G. Huffman
- 64. G. Jacobson
- 65. H. Jory
- 66. J. Moran
- 67-69. J.F. Shively
- 70. A. Staprans
- 71. D. Stone
- 72. R. Symons
- 73-75. R.M. West